

## DARK MATTER AND GRAVITATIONAL LENSING

Y. MELLIER

*Institut d'Astrophysique de Paris, 98 bis boulevard Arago  
75014 Paris, France (mellier@iap.fr)  
Observatoire de Paris, DEMIRM, 61 avenue de l'Observatoire,  
75014 Paris, France*

F. BERNARDEAU

*Service de Physique Théorique, CE Saclay  
91191 Gif-sur-Yvette Cedex, France (fbernardeau@cea.fr)*

L. VAN WAERBEKE

*Max-Planck-Institut für Astrophysik, Karl Schwarzschild-Str. 1  
85740 Garching, Germany (waerbeke@mpa-garching.mpg.de)*

The last decade has shown a considerable development of gravitational lensing for cosmology because it probes the amount and the nature of dark matter, and provides information on the density parameter  $\Omega$ , the cosmological constant  $\Lambda$  and the Hubble constant  $H_0$ . Therefore, gravitational lensing can constrain the cosmological scenario which gave birth to the Universe as it appears today. The ongoing programs and future projects which are developing now all over the world show that gravitational lensing is considered as a major cosmological tool for the coming years as well. In this review, we summarize some of the most recent advances in the fields relevant for the dark matter issue. We will focus on the microlensing, the arc(let)s and the weak lensing studies. The possibility to check the existence of a non-zero  $\Lambda$  is presented elsewhere (see Fort et al. contribution).

### 1 Introduction

The present-day structuration of the Universe likely formed from gravitational condensations of primordial fluctuations. In a homogeneous and isotropic universe, the growth and the late evolution of these fluctuations depend on the amount of mass-energy presents in the Universe and the nature of its matter content. The former is described by the cosmological parameters  $\Omega$  and  $\Lambda$ , whereas its nature can be inferred from the shape of the power spectrum of the initial fluctuations and the amount of baryonic matter we can observe today. These crucial quantities are then among the most challenging observing targets for the end of this century, and motivated also the launches of MAP and Planck-Surveyor by the beginning of 2000.

The large variety of observational techniques applied over a wide range of dynamical systems shows compelling evidence that most of them are dominated by invisible matter. Furthermore, it seems that the dark matter fraction

increases with the mass range of the systems. The amount of dark matter deduced from these studies leads to the conclusions that (1) dark matter is the main component of the Universe, (2) the visible mass does not fully account for the baryonic mass permitted from the theoretical expectations of the Big Bang Nucleosynthesis (BBN), allowing part of the dark matter to be baryonic, (3) on the other hand, if the mass-to-light ratios inferred from observations are correct, dark matter cannot be only baryonic.

There is still room for controversy on these conclusions because the measurements of the amount and the distribution of the matter are *indirect*: (1) 2- and 3-dimension galaxy surveys only depict the distribution of *light*; (2) the mass of gravitational systems are not simply inferred because assumptions on the geometry of their mass and light distribution profiles and on their dynamical stage are necessary. Some of these hypotheses are much debated. (3) Finally, the dynamical studies of large-scale galaxy flows which map the large-scale mass distribution of the Universe are not yet conclusive because of the poor quality of the catalogs.

In fact, the rotation curves of spiral galaxies seem to give by far the most robust estimates of the total mass of galaxies. Although the mass-to-light ratios inferred for these galaxies requires that their halos are dominated by dark matter, the amount needed is compatible with the upper limit of the baryon fraction deduced from BBN, and does not require that halos have non-baryonic content. Hence, the search for the nature of dark matter in galaxies as well as for new robust mass estimators is important.

Gravitational lensing effects can directly probe deflecting masses and can determine without ambiguity the amount of matter present along the line-of-sight. Its astrophysical interest only raised after the discoveries of the first multiply imaged quasar<sup>1</sup>, the gravitational arcs<sup>2, 3, 4</sup> and the arclets<sup>5</sup>. But the on-going massive monitoring of microlensing events and the development of large programs for mapping the large-scale structures by using weak lensing make gravitational lensing effect one of the most promising tools to address some cosmological issues of the next ten years. This review only focus on the recent results relevant to dark matter issue. Section 2 summarizes the fundamental concepts and equations of gravitational lensing. In section 3, the latest microlensing experiments are presented. Sections 4 and 5 are devoted to investigations of clusters of galaxies and section 6 to the promising investigation of large-scale structures.

## 2 The equations of lensing

In presence of a gravitational field, due to the local modification of the geodesics, a background source located at the apparent position,  $\vec{\theta}_S$ , appears on the sky at the new apparent position  $\vec{\theta}_I$  in presence of a gravitational field. The lensing equation relates these apparent position to the deflection angle  $\vec{\alpha}$ :

$$\vec{\theta}_S = \vec{\theta}_I - \vec{\alpha}(\vec{\theta}_I) = \vec{\theta}_I - \vec{\nabla}_{\vec{\theta}_I} \varphi = \vec{\theta}_I - \frac{2}{c^2} \frac{D_{ls} D_{ol}}{D_{os}} \int \vec{\nabla}_{\vec{\theta}_I} \Phi(\vec{\theta}_I) dz, \quad (1)$$

where  $\varphi$  is the projected lensing potential,  $\Phi$  the 3-dimension newtonian potential, and the  $D_{ij}$  are the angular distances with respect to the observer ( $o$ ), the source ( $s$ ) and the lens ( $l$ ). The  $D_{ij}$  express part of the dependence of the lensing equation with the cosmological parameters (another dependence with  $\Omega$  comes from the potential  $\Phi$  of the Poisson equation). The deformation of a beam is given by the Jacobian of the mapping between the source and the image planes, namely the amplification matrix  $A$ , whose terms are

$$A_{ij} = \left( \delta_{ij} - \frac{\partial \alpha_i(\theta)}{\partial \theta_j} \right) = \left( \delta_{ij} - \frac{\partial^2 \varphi(\theta)}{\partial \theta_i \partial \theta_j} \right). \quad (2)$$

$A$  is usually expressed with the convergence  $\kappa$ , the isotropic term of the magnification, and the gravitational shear  $\gamma = \gamma_1 + i \gamma_2$ , the anisotropic term:

$$A = \begin{pmatrix} 1 - \kappa - \gamma_1 & -\gamma_2 \\ -\gamma_2 & 1 - \kappa + \gamma_1 \end{pmatrix}, \quad (3)$$

where

$$\kappa = \frac{1}{2} \nabla^2 \varphi = \frac{\Sigma}{\Sigma_{\text{crit.}}}; \quad \gamma_1 = \frac{1}{2} (\varphi_{,11} - \varphi_{,22}); \quad \gamma_2 = \varphi_{,12}. \quad (4)$$

$\Sigma$  is the projected mass density and  $\Sigma_{\text{crit.}} = (c^2 / 4\pi G)(D_{os}/(D_{ol}D_{ls}))$  is the critical mass density for which a light beam emitted by a source would exactly focus on the observer plane.

The total magnification is  $\mu = 1/((1 - \kappa)^2 - |\gamma|^2)$ . Strong magnification events (arcs, microlensing) correspond to cases where  $\mu$  diverges to infinity. At these positions, image multiplications and strong magnification/distortion occur. For simple lens configurations, the location of the infinite amplification in the image plane can be easily computed. They are called critical lines and the corresponding positions in the source planes are the caustic lines. Despite the transient nature of some microlensing events, giant arcs and microlensing events are the same physical phenomenon. They have different applications because of the different scales involved in each case. Microlensing is perfectly

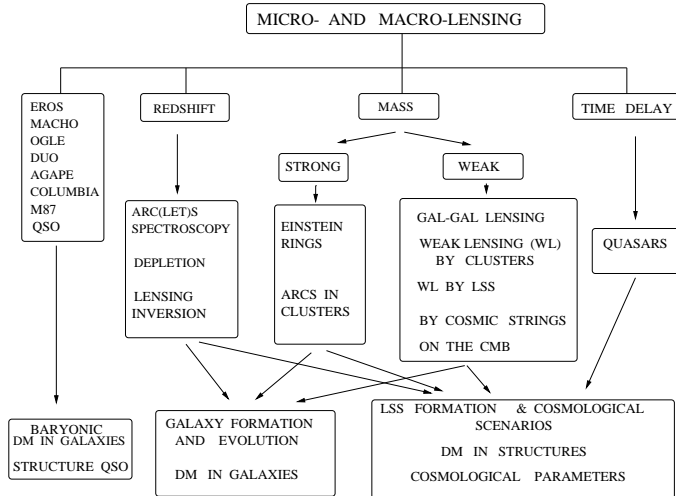


Figure 1: Some applications of gravitational lensing effects in cosmology. The left-hand box summarizes the microlensing project. COLUMBIA is the pixel monitoring project of M31 done at KPNO and VATT. M87 is a similar project on M87 done with the HST.

adapted to local events of stars, whereas arc(let)s are expected in galaxies or clusters. The weak lensing regime corresponds to a natural extension of arc(let)s where  $\kappa$  and  $\gamma$  become smaller than 1. The weak lensing regime is observed on extended sources and is well suited to study large-scale structures from the correlated alignment of background galaxies. In fact, since the lensing equation relates mass distribution and cosmological distances, gravitational lensing can be used in various contexts and has a large number of applications, as it is shown in figure 1.

### 3 Microlensing and the baryonic content of the spiral galaxies

For a single point-mass deflector with mass  $M_{lens}$ , the critical line is a circle whose radius is called the Einstein radius and writes

$$R_e = \sqrt{\frac{4GM_{lens}}{c^2} \frac{D_{ol}D_{ls}}{D_{os}}} . \quad (5)$$

A light beam approaching the lens with an impact parameter  $b$  form two images, separated by

$$\theta_{1,2} = \sqrt{b^2 + 4R_e^2} = R_e \sqrt{1 + \frac{4}{u^2}}, \quad (6)$$

where  $u = b/R_e$ . The total amplification of the two images writes

$$A = \frac{u^2 + 2}{u\sqrt{u^2 + 4}}. \quad (7)$$

Microensing eventually occurs when  $\theta_{1,2}$  is smaller than the angular resolution of telescopes. For the observer, the images are merged and only a strong point-like amplification is observed. As an example, for the EROS1/2 or MACHO experiments on Magellanic Clouds, the angular separation of images is about 1 milliarcsecond which is far below the best resolutions obtained with ground based telescopes or the HST.

In practice, microlensing events are extremely rare. However, Paczyński<sup>6</sup> pointed out that if galactic halos are formed with compact objects, they move within the galactic potential well and eventually can cross light beams of background stars. Transient microlensing events may thus occur and can be observed if millions of stars are followed up simultaneously during a long period. For compact lenses moving with velocity  $v(t)$  the magnification event spreads over a time scale  $\Delta t = R_e/v(t)$ . Hence, the typical time-scale of microlensing events is proportional to  $\sqrt{M_{lens}}$  and this property can be used to probe the mass distribution of compact deflectors.

Paczyński's suggestion inspired numerous new projects with the aim to provide on a short time scale the baryon fraction of our Galaxy and possibly of extragalactic systems. Table 1 summarizes the present-day results. We only report single events, so binary-lenses as the one discovered by Alard et al.<sup>7</sup> are not included. The last EROS2 result is the most recent of the table<sup>8</sup>.

The conclusions of EROS1 and MACHO monitorings are similar and rule out the possibility that the halo content of our Galaxy has more than 20% of compact objects with masses ranging between  $\approx 10^{-7} M_\odot$  and  $0.02 M_\odot$ . On the other hand, the statistical distribution of the events detected in the bulge of the Galaxy is compatible with a Salpeter mass distribution with masses ranging between  $0.08 M_\odot$  and  $0.6 M_\odot$ . Complementary results by Crotts & Tomaney<sup>9</sup> in M31 seem to rule out also compact objects with mass between  $0.003$  and  $0.08 M_\odot$  in the outer bulge and the inner disk of this galaxy, whereas their 6 events have typical signatures expected for  $\approx 1.0 M_\odot$  objects.

The present-day results of the microlensing experiments are puzzling and address new questions on the nature of the low-mass objects in the Galaxy. The

Survey	Target	Origin	Nb of Events	Mass Range of the Lens
EROS1	LMC/SMC	France	2	$\approx 0.15 M_{\odot}$
MACHO	LMC/SMC	USA/Australia	6	$\approx 0.3 - 0.5 M_{\odot}$
	Galaxy (bulge)	USA/Australia	$\approx 100$	$0.08 - 0.6 M_{\odot}$
OGLE	Galaxy (bulge)	USA/Poland	18	$0.08 - 0.6 M_{\odot}$
DUO	Galaxy (bulge)	France	13	$0.08 - 0.6 M_{\odot}$
AGAPE	M31	France	0	–
KPNO	M31	USA	6	$\approx 1.0 M_{\odot}$
EROS2	LMC/SMC	France	1	$0.85 - 8.7 M_{\odot}$
	Galaxy (bulge)	France	–	–

Table 1: The microlensing surveys. AGAPE and the KPNO/VATT experiments use pixel monitoring since stars cannot be resolved. AGAPE has not finished yet the data processing. A program on M87 with the HST is in project.

average mass of the objects detected in the direction of the LMC and SMC is  $0.5 M_{\odot}$ . Assuming a simple mass distribution for the halo it is then possible to infer their projected number-density and to predict that a (small) amount of such objects should be detected in the Hubble Deep Field. However, negative results have been reported so far<sup>10</sup>. Similarly, although the mass function of objects in the direction of the bulge looks like a Salpeter mass distribution with masses ranging between  $0.08 M_{\odot}$  and  $0.6 M_{\odot}$ , the deepest star counts impose strong limits on their number-density and cannot explain more than 50% of the events. In both cases, a significant fraction of the objects responsible for microlensing events seems somewhat unusual.

It is possible that the compact lenses are red-dwarfs, but they cannot account for more than 50% of the halo. White-dwarfs seem unprobable because their progenitors have not been detected, though they should be visible at high-redshift on the deepest astronomical observations<sup>11</sup>. But there are now crucial issues on the existence of a large amount of brown dwarfs in our halo in order to explain the flat rotation curve of our Galaxy. So, even if new fascinating objects are discovered from the microlensing experiments, they do not provide evidences that huge baryonic halos of dark matter exist around spiral galaxies. On the other hand, it seems impossible to abandon the idea that galaxies do have dark halos. Specific cases of Einstein-ring configurations by galaxies<sup>12</sup> and recent galaxy-galaxy lensing analyses by Brainerd et al.<sup>13</sup> and Griffiths et al.<sup>14</sup> indicate that mass-to-light ratios of galaxies are larger than 10 and that their halos could extend up to  $\approx 100 h^{-1}\text{kpc}$ .

Figure 2: HST images of arcs: top left is A2218, center left: A2390, bottom left: MS2137-23, top right: A370, middle right: Cl2244-02, bottom right: Cl0024+17.

#### 4 Arc(let)s in clusters of galaxies

Giant arcs form at the points where  $\mu$  is (close to) infinite. From the position of the source with respect to the caustic lines, one can explain typical lensing configurations where arcs form from the merging of two, three, or even more images, as well as more surprising shapes like radial arcs and “straight arcs”<sup>15, 16</sup>.

Typical lensing cases have been observed in rich clusters of galaxies, like in MS2137-23<sup>17</sup>, A370<sup>18</sup>, AC114<sup>19</sup>, or A2218<sup>20</sup>. In some cases the positions and shapes of images have been predicted and confirmed later which gives strong confidence in the reconstructed mass distribution. But the most impressive results were provided by using the HST images (see figure 2). The outstanding image quality of the HST reveals small details in each arc that can be used to recognize the multiply-imaged galaxies by eye<sup>21, 22, 23, 24, 25</sup>.

Arcs constrain the central mass distribution of clusters of galaxies on a scale of  $\approx 500h^{-1}\text{kpc}$  (see table 2). They have demonstrated that their mass-to-light ratio on this scale ranges between 100 and 300 which definitely shows that clusters of galaxies are dominated by dark matter and that  $\Omega$  inferred from arcs lies in the range 0.15 to 0.3. The lens modelling shows that on  $\approx 100$  kpc scale, dark matter closely follows the geometry of the light distribution associated with the brightest cluster members. Furthermore, since arcs occur when  $\Sigma/\Sigma_{\text{crit.}} > 1$ , clusters of galaxies must be much more concentrated than it was expected from their galaxy and X-ray gas distributions. But the occurrence of arcs is also enhanced by the existence of additional clumps observed in most of the rich clusters which increases the shear substantially<sup>26</sup>. The direct observations of substructures by using HST images of lensing-clusters confirm that clusters are dynamically young systems. Most of these clumps are centered around bright early-type galaxies (see figure 2). Natarajan & Kneib<sup>27</sup> and Geiger & Schneider<sup>28</sup> proposed to use these images in order to infer the mass of halos of galaxies in clusters. The benefit of additional convergence by the extended halo of the lensing-cluster enhances the galaxy-galaxy lensing effect which thus can be easily detected. Though promising, no conclusive results have been raised yet, mainly because the two lensing effects (cluster and galaxy-galaxy) mix together and combine weak and strong lensing effect simultaneously which are difficult to separate.

Cluster	$\mathbf{z}_{cluster}$	Scale ( $h^{-1}$ kpc)	M/L ( $h$ )	$\mathbf{z}_{arc}$
MS2137-23 <sup>17</sup>	0.33	500	340-140	0.7-1.5
A370 <sup>18</sup>	0.37	500	> 150	0.725
C10024+17 <sup>52</sup>	0.39	500	> 200	$\approx 0.9$
C10024+17 <sup>21</sup>	0.39	500	> 200	$\approx 0.9$
A2218 <sup>20, 22</sup>	0.18	1000	200	0.702 & 1.034
A2390 <sup>53</sup>	0.23	400	250	0.913

Table 2: Mass model inferred from modelling of some spectacular arcs. The scales are expressed in  $h_{100}^{-1}$  Kpc.

## 5 Weak lensing by clusters of galaxies

Far from the critical lines, light beams of background galaxies crossing lensing-clusters are only weakly magnified, but still produce a small increase of their ellipticity in the direction perpendicular to the gradient of the projected potential (shear). The effect on each individual galaxy is much weaker than the average intrinsic ellipticity of the sources but it is possible to use this coherent polarization pattern statistically in order to recover the mass distribution of the lens.

The population of weakly distorted galaxies probes the distortion induced by the lens on the projected space. The projected mass density  $\Sigma$  can be recovered by using the shape parameters of the images  $M^I$  which are related to the shape parameters of the sources  $M^S$  by the equation,

$$M^S = AM^I A, \quad (8)$$

where  $M$  are the second moment of galaxies and  $A$  the magnification matrix. The ellipticity of the sources  $\epsilon_S = (a_S - b_S)/(a_S + b_S)$ , where  $a_S$  and  $b_S$  are the major and minor axis respectively, is related to ellipticity of the images  $\epsilon_I$  and the complex shear  $g$  as follows:

$$\epsilon_S = \frac{\epsilon_I - g}{1 - g^* \epsilon_I}; \quad g = \frac{\gamma}{1 - \kappa}. \quad (9)$$

The sources are randomly distributed, hence their averaged intrinsic ellipticity is  $\langle \epsilon_S \rangle = 0$  which implies that

$$g = \langle \epsilon_I \rangle. \quad (10)$$

In the weak lensing regime,  $(\kappa, \gamma) \ll 1$ , and the relations between the physical ( $\gamma$ ) and observable ( $\epsilon_I$ ) quantities reduce to,

$$\langle \epsilon_I \rangle = \gamma . \quad (11)$$

The projected mass density  $\Sigma$  of the lens is recovered from the distortion field by using Eq.(11) and the integration of Eq.(4)<sup>29, 30, 31, 32</sup>:

$$\kappa(\vec{\theta}_I) = \frac{-2}{\pi} \int d^2\theta \gamma(\vec{\theta}_I) \frac{\chi(\vec{\theta} - \vec{\theta}_I)}{(\vec{\theta} - \vec{\theta}_I)^2} + \kappa_0 ; \quad \chi(\vec{\theta}) = \left( \frac{\theta_1^2 - \theta_2^2}{\theta^2} + i \frac{2\theta_1\theta_2}{\theta^2} \right), \quad (12)$$

where  $\kappa_0$  is an integration constant.

Table 3 summarizes results on clusters for which mass reconstruction from lensing inversion have been done. When compared with mass distribution inferred from strong lensing, there is a clear trend towards an increase of  $M/L$  with scale. Bonnet et al.<sup>33</sup> find  $M/L$  close to 600 at  $2.5 h^{-1}\text{Mpc}$  from the cluster center, and on  $1-h^{-1}\text{Mpc}$  scale  $M/L$  ranges between 150 and 400, that is  $0.2 < \Omega < 0.5$ . This large spread is due to important uncertainties. In particular, the redshift distribution of the background sources is poorly known. Though it is not a critical issue for nearby clusters ( $z_l < 0.2$ ), because then  $D_{os}/D_{ls} \simeq Cste$ , it could lead to large mass uncertainties for more distant clusters, as for MS1054 which is at  $z = 0.83$ <sup>34</sup>. The other critical point is the measurement of ellipticities as low as 1% on faint objects which is extremely difficult in practice.

Even if the redshift of the sources were known, it is not sufficient to get the absolute value of the mass distribution, because structures with constant mass density eventually intercepting the beam do not change the shear map. This issue is expressed by the unknown integration constant  $\kappa_0$  in Eq.(12). The degeneracy may be broken if one measures the magnification  $\mu$ , by comparing properties of lensed and unlensed sources. Broadhurst et al.<sup>35</sup> proposed to compare the number count  $N(m, z)$  and/or  $N(m)$  in a lensed and an unlensed field to measure  $\mu$  (see Fort, this conference). This method was applied on the cluster by Broadhurst<sup>36</sup> in A1689 and by Fort et al.<sup>37</sup> on Cl0024+17 and A370. The magnification may also be determined by the changes of the image sizes at fixed surface brightness<sup>38</sup>. However, even if the measurement of the magnification is an exiting approach to probe the lensing effects indepently of the measure of the shear, it is still extremely difficult to get its amplitude accurately. The number counts method is sensible to the Poisson noise and the intrinsic clustering. The surface brightness method suffers of the lack of precise operational definition and of the dilution of light due to the seeing.

Cluster	$z_{cluster}$	Scale ( $h^{-1}$ kpc)	M/L ( $h$ )	$z_{source}$
1455+22 <sup>54</sup>	0.26	500	460	–
Cl0016+16 <sup>54</sup>	0.55	500	430	–
MS1224 <sup>51</sup>	0.33	500	800	1-2
Cl0024 <sup>33</sup>	0.39	2500	600	1-2
A1689 <sup>59</sup>	0.18	1000	400	0.9
A1689 <sup>47</sup>	0.18	500	> 200	1-2
A1689 <sup>36</sup>	0.18	500	> 200	1-2
A2218 <sup>57</sup>	0.18	400	440	0.7 & 1-2
A2390 <sup>58</sup>	0.23	1000	320	1-2
Cl0939 <sup>55</sup>	0.41	400	200	0.6-1
MS1054 <sup>34</sup>	0.83	400	1600 580 350	<1 =1.5 =3.

Table 3: Example of mass reconstruction obtained from weak lensing inversion. The mass-to-light ratios are higher than from giant arc (see table 2). The uncertainty in the case of MS1054 expresses the dependence of mass with the redshift of the sources.

## 6 The matter distribution on very large scale

The direct observation of the mass distribution on scales larger than  $10 h^{-1}\text{Mpc}$  (or  $\approx 1$  square degree) is a natural step beyond clusters of galaxies and is actually the main goal in cosmology for the next decade. Two observational directions are now being investigated. In the first one, the statistical properties of weakly lensed background galaxies on degree scales are investigated in order to build maps of the projected mass-density of large-scale structures from the gravitational shear, and to constrain the cosmological parameters and the projected power spectrum of initial fluctuations. In the second one, the gravitational shear on small scales ( $< 10$  arcminutes) induced by non-linear systems is analyzed in order to constrain the cosmological parameters and the projected power spectrum as well, and to correct quasar statistics from magnification biases.

At very large scale, the lenses are not individually identified, but viewed as a random population affecting the shape of the galaxies. Each object along a given line of sight may play simultaneously the role of a lens for background galaxies and of a source for foreground systems, so that the efficiency depends on the redshift distribution of the whole population. The shear measured of each field is filtered at a given angular scale so that a signal of cosmological

Figure 3: Simulation of shear induced by large-scale structures. The left panel shows a  $(256 \text{ Mpc})^3$  box indicating the location of matter. The filaments are large-scale structures which grew from a uniform distribution and an initial power spectrum  $P(k) = k^{-1}$ , evolving under the adhesion approximation. The right panel shows thin straight lines which illustrate the local orientation and intensity of the shear.

interest can be extracted. For a filtering scale of about one degree, the structures responsible of the gravitational shear being at a redshift of about 0.4 are expected to be on scales above  $10 h^{-1} \text{ Mpc}$ , that is in a regime where their properties can be easily predicted with the linear or perturbation theory. Blandford et al. <sup>39</sup>, Miralda-Escudé <sup>40</sup> and Kaiser <sup>41</sup> argued that the projected power spectrum should be measurable with such a method provided shape parameters are averaged on the degree scale, as it is illustrated on figure 3 <sup>42</sup>. Further studies using various cosmologies, various statistics and more realistic ellipticity and redshift distributions have been done recently in the perspective of wide fields surveys <sup>43, 44, 45, 46</sup>.

Using the Perturbation Theory, Bernardeau et al. <sup>44</sup> have analyzed the statistical properties of the gravitational shear averaged on degree scale. Assuming a power-law for the power spectrum, they have shown that the observation of about 25 such fields permits to recover the projected power spectrum and  $\Omega$  independently, with 10% accuracy, by using the variance,  $\langle \kappa_\theta^2 \rangle$ , and the skewness,  $\langle \kappa_\theta^3 \rangle / \langle \kappa_\theta^2 \rangle^2$ , of the probability distribution function of the local convergence in the sample. These moments write,

$$\langle \kappa_\theta^2 \rangle \propto P(k) \Omega^{1.5} z_s^{1.5} ; \frac{\langle \kappa_\theta^3 \rangle}{\langle \kappa_\theta^2 \rangle^2} \propto \Omega^{-0.8} z_s^{-1.35} \quad (13)$$

where  $\theta = 30'$  is the scale where the convergence  $\kappa$  is averaged,  $P(k)$  is the projected power spectrum of the dark matter and  $z_s$  is the averaged redshift of sources. Bernardeau et al. notice that the product of these two quantities provides an information on  $\Omega$  and  $P(k)$  regardless the redshift distribution of sources which is basically unknown for the faint galaxies.

Recently, Jain & Seljak <sup>48</sup> have investigated the effect of the non-linear evolution of the power spectrum on the amplitude of the variance. They show that at scales above 30 arcminutes the variance is not much affected, but at scales below 2 arcminutes the non-linear structures induce a significant increase of the expected signal for the shear. Its amplitude is expected to be between 2% and 5% depending on cosmology. In fact, this ‘‘cosmic shear’’ may have been detected already by Fort et al. <sup>49</sup> and Schneider et al. <sup>50</sup>. If it is so, we could be already able to obtain a preliminary value for  $\Omega$  very soon by using

weak lensing effects.

## 7 Conclusions

Microlensing surveys have shown that the existence of a baryonic halo dominated by brown dwarfs around our Galaxy is not confirmed. However, galaxy-galaxy lensing and Einstein rings suggest that galactic halos of dark matter are present. Instead, microlensing events reveal a new population of compact star-like objects may exist in our Galaxy. On the other hand, studies of arc(let)s and weak lensing in clusters show that  $\Omega > 0.2$  is almost certain and provide evidence that  $0.2 < \Omega < 0.6$  on scales below  $2.5 h^{-1}$  Mpc. The next decade will provide important constraints on  $\Omega$  and  $P(k)$ , as well as first maps of mass-density of the Universe on  $100h^{-1}$  Mpc scales regardless the light distribution. This is an enthusiastic period for gravitational lensing applications to cosmology.

## Acknowledgments

We thank B. Fort, P. Schneider and S. Seitz for fruitful discussions and enthusiastic collaborations. We thank B. Fort, B. Geiger and J.-P. Kneib for careful reading of the manuscript.

## References

1. Walsh, D., Carswell, R.F., Weymann, R.J. 1979, *Nature*, 279, 381.
2. Soucail, G., Fort, B., Mellier, Y., Picat, J.-P. 1987, *A&A* 172, L14.
3. Soucail, G., Mellier, Y., Fort, B., Mathez, G., Cailloux, M. 1998, *A&A* 191, L19.
4. Lynds, R., Petrosian, V. 1986, *BAAS* 18, 1014.
5. Fort, B., Prieur, J.-L., Mathez, G., Mellier, Y., Soucail, G. 1988, *A&A* 200, L17.
6. Paczynski, B. 1986, *ApJ* 304, 1.
7. Alard, C., Mao, S., Guibert, J. 1995, *A&A* 300, L17.
8. Palanque-Delabrouille, N. 1997, PhD Thesis, Université de Paris 7 and University of Chicago.
9. Crotts, A. P. S., Tomaney, A. B. 1996, *ApJ* 473, 87.
10. Flynn, C., Gould, A., Bahcall, J. N. 1996, *ApJ* 466, L55.
11. Charlot, S., Silk 1995, *ApJ* 445, 124.
12. Kochanek, C. S. 1995, *ApJ* 445, 559.
13. Brainerd, T. G., Blandford, R. D., Smail, I. 1996, *ApJ* 466, 693.

14. Griffiths, R. E., Casertano, S., Im, M., Ratnatunga, K. U. 1996, ApJ 471, L15.
15. Fort, B., Mellier, Y. 1994, A&AR 5, 239, 292.
16. Narayan, R., Bartelmann, M. 1996, astro-ph/9606001
17. Mellier, Y., Fort, B., Kneib, J.-P. 1993, ApJ 407, 33.
18. Kneib, J.-P., Mellier, Y., Fort, B., Mathez, G. 1993, A&A 273, 367.
19. Smail, I., Couch, W., Ellis, R. S., Sharples, R. M. 1995, ApJ 440, 501.
20. Kneib, J.-P., Mellier, Y., Pelló, R., Miralda-Escudé, J., Le Borgne, J.-F., Böhringer, H., Picat, J.-P. 1995, A&A 299, 168.
21. Wallington, S., Kochanek, C. S., Koo, D. C. 1995, ApJ 441, 58.
22. Kneib, J.-P., Ellis, R. S., Smail, I., Couch, W., Sharples, R. M. 1996, ApJ 471, 643.
23. Hammer, F., Teyssandier, P., Shaya, E. J., Gioia, I. M., Luppino, G. A. 1996, astro-ph/9610207.
24. Natarajan, P., Kneib, J.-P., Smail, I., Ellis, R. S. 1997, astro-ph/9706129.
25. Seitz, S., Saglia, R. P., Bender, R., Hopp, U., Belloni, P., Ziegler, B. 1997, astro-ph/9706023.
26. Bartelmann, M. 1995, A&A 299, 661.
27. Natarajan, P., Kneib, J.-P. 1996, MNRAS 287, 833.
28. Geiger, B., Schneider, P. 1997, astro-ph/9707044.
29. Kaiser, N., Squires, G. 1993, ApJ 404, 441
30. Seitz, C., Schneider, P. 1995, A&A 302, 9
31. Schneider, P. 1995, A&A, 302, 639
32. Seitz, S., Schneider, P. 1996, A&A 305, 388
33. Bonnet, H., Mellier, Y., Fort, B. 1994, ApJ 427, L83.
34. Luppino, G., Kaiser, N. 1997, ApJ 475, 20.
35. Broadhurst, T., Taylor, A. N., Peacock, J. 1995, ApJ 438, 49.
36. Broadhurst, T. 1995, astro-ph/9511150.
37. Fort, B., Mellier, Y., Dantel-Fort 1997, A&A 321, 353.
38. Bartelmann, M., Narayan, R. 1995, ApJ 451, 60.
39. Blandford, R.D., Saust, A.B., Brainerd, T.G., Villumsen, J.V. 1991, MNRAS, 251, 600
40. Miralda-Escudé, J. 1991, ApJ, 370, 1.
41. Kaiser, N. 1992, ApJ 388, 272.
42. Mellier, Y., Van Waerbeke, L., Bernardeau, F., Fort, B. 1997, *Neutrinos, Dark Matter and the Universe*. Proceeding of the XVIII<sup>ieme</sup> Rencontres de Blois. T. Stolarczyk, J. Tran Thanh Van, F. Vannucci eds.
43. Villumsen, J. V. 1996, MNRAS 281, 369.
44. Bernardeau, F., Van Waerbeke, L., Mellier, Y. 1997, A&A 322, 1.
45. Stebbins, A. 1996, astro-ph/9609149.

46. Kaiser, N. 1996, astro-ph/9610120.
47. Kaiser, N. 1995, astro-ph/9509019.
48. Jain, B., Seljak, U. 1997, ApJ 484 560.
49. Fort, B., Mellier, Y., Dantel-Fort, M., Bonnet, H., Kneib, J.-P. 1996a, A&A 310, 705.
50. Schneider, P., Van Waerbeke, L., Mellier, Y., Jain, B., Seitz, S., Fort, B. 1997, astro-ph/9705122.
51. Fahlman, G., Kaiser, N., Squires, G., Woods, D. 1994, ApJ 437. 56.
52. Kassiola, A., Kovner, I., Fort, B. 1992, ApJ 400, 41.
53. Pierre, M., Le Borgne, J.-F., Soucail, G., Kneib, J.-P. 1996, A&A 311, 413.
54. Smail I, Ellis, R. S., Fitchett M. 1994, MNRAS 270, 245.
55. Seitz, C., Kneib, J.P., Schneider, P., Seitz, S. 1996, A&A 314, 707.
56. Squires, G., Neumann, D.M., Kaiser, N., Arnaud, M., Babul, A., Böhringer, H. Fahlmann, G., Woods, D. 1997, ApJ 482, 648.
57. Squires, G., Kaiser, N., Babul, A., Fahlmann, G., Woods, D., Neumann, D.M., Böhringer, H. 1996, ApJ 461, 572.
58. Squires, G., Kaiser, N., Fahlman, G., Babul, A., Woods, D. 1996, ApJ 469, 73.
59. Tyson, J.A., Fisher, P. 1995, ApJ 349, L1.